

Resolved Stellar Populations
ASP Conference Series, Vol. TBA, 2005
D. Valls-Gabaud & M. Chavez (eds)

IMF biases and how to correct them

J. Maíz Apellániz^{1,2}, L. Úbeda¹, N. R. Walborn¹, and E. P. Nelan¹

¹ *Space Telescope Science Institute, 3700 San Martin Drive, Baltimore, MD 21218, U.S.A.*

² *Space Telescope Division, European Space Agency, ESTEC, Noordwijk, Netherlands*

Abstract. We discuss possible sources of biases in the determination of the initial mass function (IMF) introduced by the binning of the data, the uncertainty in the determinations of masses, and the existence of unresolved multiple systems. Those three effects tend to produce IMFs that are flatter than the real one. We analyze the importance of each effect and suggest techniques that minimize or eliminate the biases. We also report the detection of the first astrometric binary system composed of two very-early O-type stars, HD 93129 A.

1. Introduction

In order to obtain the mass function of a stellar population from photometric data one starts by placing the stars in a color-magnitude or in a theoretical (temperature-luminosity) HR diagram along with the evolutionary tracks and the corresponding isochrones. For a simple population one can then find the appropriate isochrone and obtain the masses for each star. For a complex star formation history, one has to obtain the full transformation from temperature and luminosity (or color and magnitude) to mass and age. The number of stars as a function of mass (corrected for age effects if necessary) can then be used to obtain the initial mass function (or IMF).

A number of problems and biases can arise along the way to obtaining the true IMF due to the oversimplification of the assumptions (e.g. using isochrone fitting for a population with an age spread), the existing intrinsic degeneracies (e.g. the complicated topology of evolutionary tracks, metallicity effects, and rotation can make two stars of different masses and ages have the same temperature and luminosity), as well as for other reasons. In this work we will analyze three sources of systematic effects: the numerical bias introduced by the use of constant-size bins for the fitting of the IMF, the “mass diffusion” from low to high masses due to photometric uncertainties, and the existence of unresolved multiples. Those three effects go in the same direction of making the measured IMF flatter than the real one and can affect different samples to different degrees, thus introducing the possibility of yielding a dispersion of measured IMF values where only a single one exists in reality.

2. Binning biases

The first type of bias we will discuss is purely numerical and affects not only IMF determinations but the fitting of any function to binned data that follows Poisson or multinomial statistics (Wheaton et al. 1995; Lucy 2000) and was analyzed by Maíz Apellániz & Úbeda (2005). Suppose we have measured the masses (m) for a set of stars to which we want to fit a power law of the form:

$$\frac{dn}{dm} = A \cdot m^\gamma, \quad (1)$$

where dn is the number of stars with mass in the interval m to $m + dm$. Integrating both sides of the equation and taking logarithms we arrive at the expression:

$$\log_{10} N_i = \log_{10} \left(\frac{A}{\gamma + 1} \cdot \left[\left(x_i + \frac{\Delta m_i}{2} \right)^{\gamma+1} - \left(x_i - \frac{\Delta m_i}{2} \right)^{\gamma+1} \right] \right), \quad (2)$$

where x_i is the mass at the center of an interval of width Δm_i that contains N_i stars. Equation 2 is the expression that can be used to derive the IMF slope, γ , by measuring the number of stars in each bin and fitting the data, which can be done by minimizing a χ^2 statistic and deriving the associated uncertainties. Since N_i follows a binomial distribution (with N being the total number of stars summed over all bins), the associated weight for bin i for the χ^2 fit is given by:

$$w_i = \frac{N_i N}{(N - N_i)(\log_{10} e)^2}. \quad (3)$$

Two warnings should be given here. The first one is that for two bins i and j , N_i and N_j are correlated because they are both part of a joint multinomial distribution (see e.g. Lucy 2000). The second and most important one is that the value of N_i that should be strictly used in Eq. 3 is the one calculated from the fit, not the one measured from the data (Wheaton et al. 1995). Otherwise, one runs into the possibility of introducing biases in the measurement of γ unless some precautions are taken because of the differences between the real and the assumed weights assigned to bins with a small number of stars in them.

Using the fit N_i instead of the data N_i for the weights requires iterating and, therefore, complicates the IMF calculation. An alternative strategy was analyzed by Maíz Apellániz & Úbeda (2005): rather than trying to find the right weights for each bin, one can select the bins in such a way that they all have similar weights and, therefore, the obtained value of γ is nearly independent of the weights themselves. In this manner, the weights derived from the data should give very similar results to the weights derived from the fit, hence eliminating the need for an iterative procedure. This strategy can be implemented by using bins with object equipartition, i.e. selecting the bins in such a way that they all have the same number of stars in them. A graphical example of the difference between constant bin-size (the standard approach to fitting binned data) and variable bin-size with object equipartition can be seen in Fig. 1.

In order to test whether variable bins provide a significant improvement over constant bins, Maíz Apellániz & Úbeda (2005) designed a series of Montecarlo

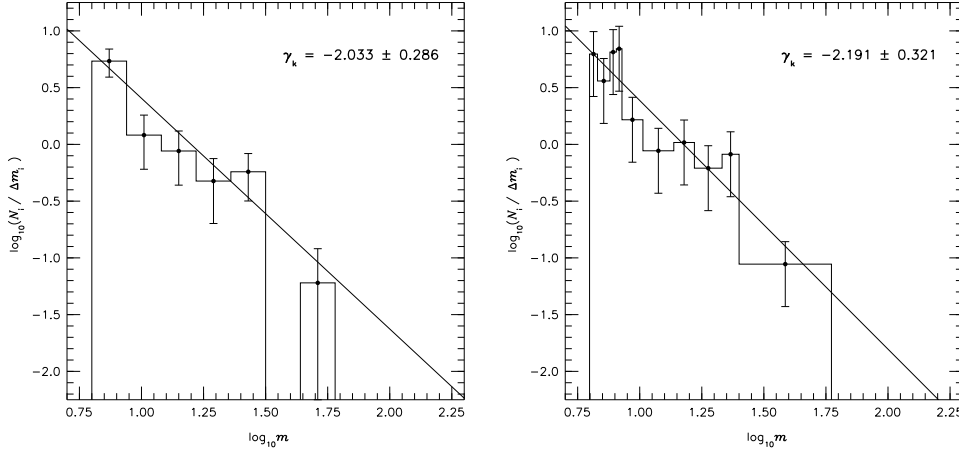


Figure 1. Comparison between the data and the fitted functions for one of the realizations with 30 stars and 10 bins for the two numerical experiments described in the text. The left panel corresponds to the first experiment (constant bin size, fixed lower and upper mass limits) while the right panel corresponds to the second experiment (variable bin size with object equipartition, lower and upper mass limits determined from the data). Note the differences in the size of the error bars between the two experiments and that the left panel plot includes four bins with zero stars.

Table 1. Normalized biases for the first experiment (constant bin size) for 3, 5, 10, 30, and 50 bins.

stars	b				
	3	5	10	30	50
30	0.376	0.655	1.181	2.393	2.986
100	0.176	0.376	0.772	2.058	2.988
300	0.121	0.224	0.430	1.384	2.200
1000	0.151	0.163	0.260	0.766	1.275

Table 2. Normalized biases for the second experiment (bin equipartition) for 3, 5, 10, 30, and 50 bins.

stars	b				
	3	5	10	30	50
30	0.110	0.134	0.180	0.264	...
100	0.047	0.046	0.071	0.143	0.161
300	0.053	0.066	0.065	0.065	0.080
1000	0.044	0.079	0.079	0.073	0.086

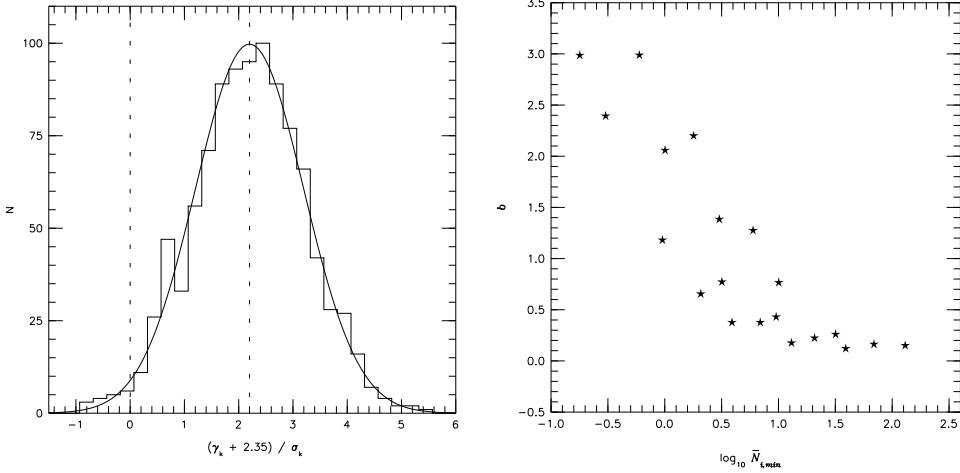


Figure 2. (left) Histogram with the distribution of $(\gamma_k + 2.35)/\sigma_k$ for the 1000 realizations of the first experiment with 300 stars and 50 bins. A Gaussian distribution with mean $b = 2.200$ and dispersion of 1.0 is also plotted for comparison. The vertical lines mark the position of 0 and of b . (right) Bias as a function of $\bar{N}_{i,\min}$ for the first experiment. Note that $\bar{N}_{i,\min}$ can be smaller than 1 because it is a property derived from the parent distribution.

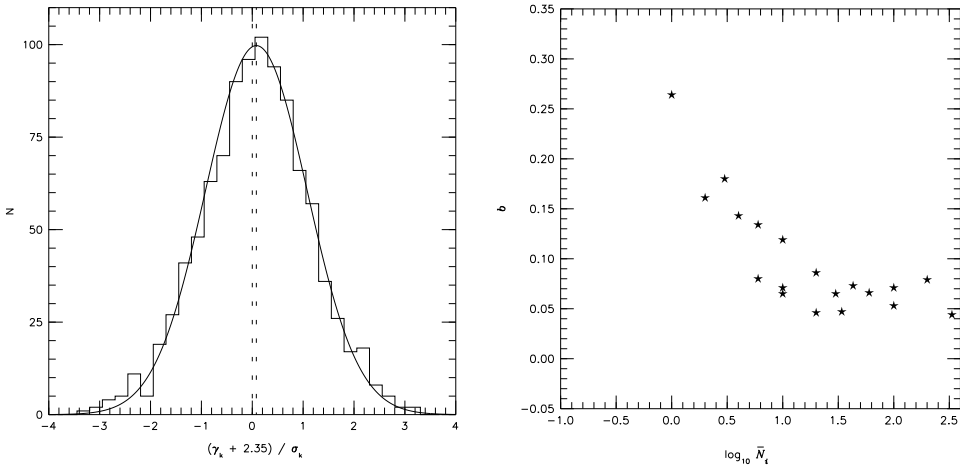


Figure 3. (left) Histogram with the distribution of $(\gamma_k + 2.35)/\sigma_k$ for the 1000 realizations of the second experiment with 300 stars and 50 bins. A Gaussian distribution with mean $b = 0.090$ and dispersion of 1.0 is also plotted for comparison. The vertical lines mark the position of 0 and of b . (right) Bias as a function of \bar{N}_i for the second experiment. Note that the vertical scale for the plot is 1/10 of that of the right panel in Fig. 2.

numerical experiments in which they also analyzed the importance of the choice of the lower and upper mass limits. The reader is referred to that article for details; here we provide a summary in Tables 1 and 2 and in Figs. 2 and 3 of two of the experiments. In the first experiment, they generated 1000 realizations from a distribution with Salpeter ($\gamma = -2.35$) slope using either $N = 30, 100, 300$, or 1000 stars. Each realization was then binned into 3, 5, 10, 30, and 50 constant-size bins and a power law was fitted using χ^2 minimization. Finally, for the 1000 realizations of each $N +$ number of bins combinations the normalized bias b was computed using the definition:

$$b = \frac{1}{1000} \sum_{k=1}^{1000} \frac{\gamma_k + 2.35}{\sigma_k}, \quad (4)$$

where σ_k is the uncertainty in γ_k derived from χ^2 minimization and the k index is used to denote the realization number. b is a sensible choice to judge the existence of biases. If $|b| \ll 1$, then the fitting method will be unbiased because it will yield values that will be larger than the real one on $\approx 50\%$ of the occasions and smaller on another $\approx 50\%$. If, on the other hand, $|b| \sim 1$ or larger, a significant bias will exist.

As seen in Table 1, significant biases exist for most $N +$ number of bins combinations when using constant bins. In the right panel of Fig. 2 we see that b is a strong function of $\bar{N}_{i,\min}$, the mean N_i in the bin with the lowest number of counts (which for constant-size bins and a Salpeter power law will be the rightmost one). Note that at least 10 stars in the rightmost bin are required for this method to yield small biases, thus making its use impractical for most applications. Also note that the bias always points in the direction of making the measured IMF flatter than what it really is and that, for a fixed number of bins, the effect is larger when there are fewer stars.

The second experiment (third in the numbering of Maíz Apellániz & Úbeda 2005) was a repetition of the first one using bin equipartition instead of constant bins. As a comparison of Tables 1 and 2 shows, the biases for the second experiment are much smaller (even for the extreme case of dividing 30 stars into 30 one-star bins, b is only 0.264). The effect is also perceptible in the right panel of Fig. 3, where the vertical scale is a factor of 10 smaller than in the equivalent panel of Fig. 2. Furthermore, the left panel of Fig 2 shows that the distribution of $(\gamma_k + 2.35)/\sigma_k$ is well approximated by a Gaussian with a dispersion of 1.0, indicating that the random uncertainties derived from χ^2 minimization can also be trusted.

We conclude that the bin equipartition strategy proposed by Maíz Apellániz & Úbeda (2005) for the fitting of power laws with Salpeter slopes yields results that (a) are nearly bias-free and (b) produce correct uncertainty estimates. On the other hand, the standard uniform-size binning introduces biases that are dependent on the number of stars per bin. The power of the equipartition technique extends to small samples, since it is possible to obtain accurate values with reasonable precisions for the IMF slope even when as few as 30 stars are available for analysis.

We would also like to point out that, given the purely numerical nature of the analysis, these results could be extended to other similar problems. For

example, the mass function for young stellar clusters can be rather well approximated by a power law with a slope of -2.0 (see e.g. Fall & Zhang 2001), which is quite close to -2.35 , so the same type of biases should be present there as well. In general, we recommend that biases be evaluated for any function fitted to binned data through χ^2 minimization by means of specific numerical experiments analogous to the ones in this article.

3. Mass diffusion

The second type of bias we will discuss is caused by photometric uncertainties and detection limits. When one tries to use photometric data to derive statistical properties of a stellar population, one finds that corrections for the undetected stars must be included in the calculation because it is easier to detect bright stars than dim ones. Such an incompleteness correction is usually handled by crowded-field photometry packages such as DAOphot (Stetson 1987) or HSTphot (Dolphin 2000) by doing experiments in which the code is run with artificial stars added and the percentage of recovered objects as a function of magnitude and color is calculated. The correction is then applied to the observed stellar statistics.

Obviously, ignoring an incompleteness correction can result in a large bias in the measurement of the IMF and this well-known fact is taken into consideration in modern works on the subject. However, a related bias which is more subtle is not always taken into account. Suppose that we observe several times a star that has a real magnitude m . Due to Poisson, detector, and background noise, in some of our observations we will measure a magnitude $m' > m$ and in others we will measure $m' < m$. If our detector is well calibrated, the first circumstance will happen 50% of the time and the second one the remaining 50%. From our analysis of the detector we should be capable of estimating from a single measurement of the star an uncertainty σ_m in such a way that $m' \pm \sigma_m$ behaves in an approximately Gaussian way, e.g. the single-measurement values m' will be within $m - \sigma_m$ and $m + \sigma_m$ for approximately 2/3 of the sample and outside $(m - 2\sigma_m, m + 2\sigma_m)$ for approximately 5% of the sample. Now, for most of the stellar mass range the IMF has a negative slope, meaning that there are more low-mass (dim) stars than high-mass (bright) ones. Therefore, if we measure a star to have magnitude m' , there should be a higher probability that its real magnitude m is dimmer than m' than that it is brighter (i.e. there are more dim stars disguised as bright ones at a given measured magnitude than bright stars disguised as dim ones) because the underlying real luminosity distribution provides more dim stars to start with. We will call this effect mass diffusion because it acts in a manner analogous to a diffusion process, smoothing a gradient by shifting objects from where they are more abundant to where they are more scarce.

Computing the correction required to eliminate mass-diffusion effects from an IMF is not straightforward because two intermediate steps are required. First, one has to translate uncertainties in the measured magnitudes and colors into uncertainties in temperature and luminosity (or bolometric magnitudes). Second, the uncertainties in the theoretical HR diagram have to be converted into uncertainties in mass. The first step involves applying extinction and bolometric

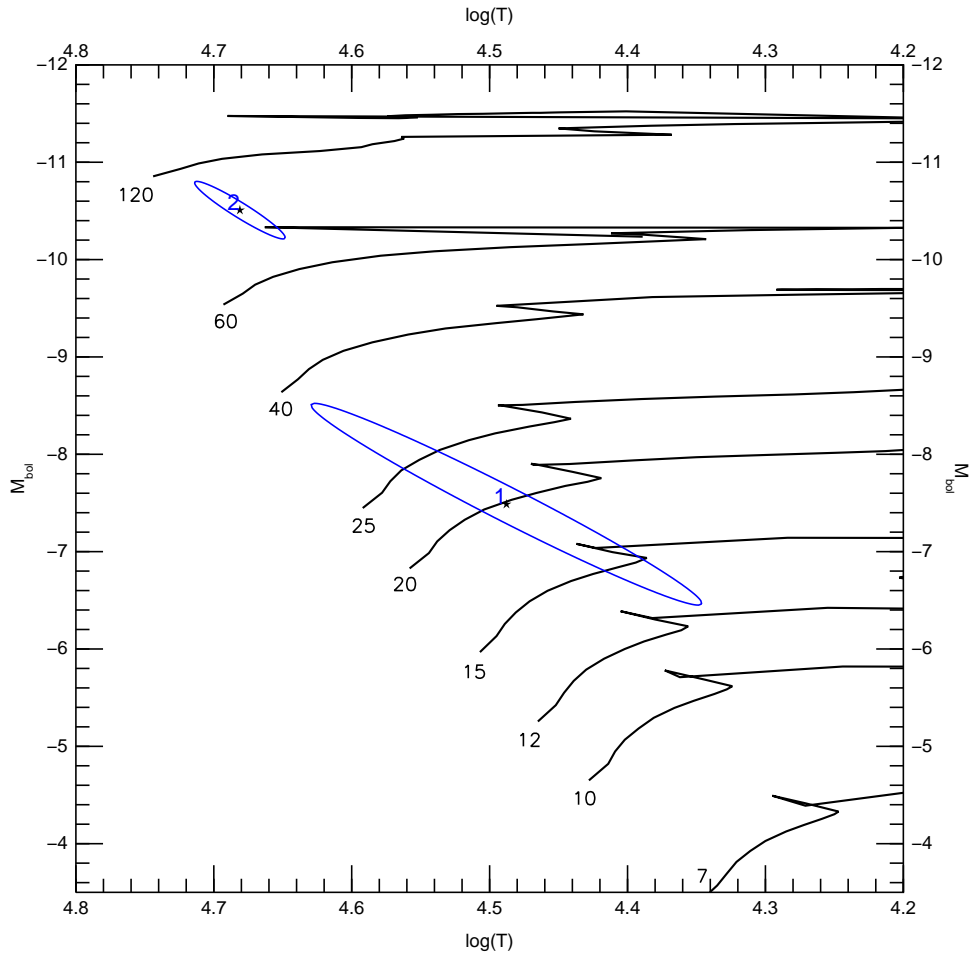


Figure 4. Converting from photometry-derived temperatures and luminosities to masses. This plot shows the temperatures and luminosities for two stars in NGC 4214 derived from HST/WFPC2 F170W+F336W+F555W+F814W photometry and their associated uncertainty ellipses. Also shown are evolutionary tracks from Maeder & Meynet (2001).

corrections and taking into consideration the correlations between them and the measured magnitudes. An example of such effects is shown in Fig. 4, where we have plotted the temperatures and bolometric magnitudes of two stars in NGC 4214 derived from multiband HST/WFPC2 stellar photometry (Úbeda et al. 2005). A strong correlation is observed between temperatures and bolometric magnitudes: most of this correlation is caused by the strong temperature dependence of the bolometric correction. The data plotted in Fig. 4 was calculated using CHORIZOS (Maíz Apellániz 2004), a code specifically designed for the task of transforming from measured magnitudes to physical properties such as temperature, age, or extinction. Note that the lower uncertainty ellipse is larger than the upper one: most of this effect is caused by the higher uncertainties in the measured magnitudes of dim stars compared to bright ones.

The second step (calculating the uncertainties for the masses) can be achieved by producing a point-to-point coordinate conversion between temperature + luminosity and mass + age (with the caveats about one-to-one correspondence previously mentioned), generating a distribution of temperatures and luminosities for each star according to its uncertainty ellipse, transforming those values into masses and ages using the conversion above, and calculating the mean and standard deviation of the derived mass distribution for each star. Those values can then be used as the mass (M_i) and its uncertainty (σ_{M_i}) for each star.

Once the masses and corresponding uncertainties have been computed for each star, one can calculate the correction due to mass diffusion in the following way. First, a function $\sigma_M(M)$ is computed from the values for the individual stars (M_i, σ_{M_i}) by fitting a simple function such as a parabola. Then, one generates a series of realizations of the IMF with different values of the slope (which we will call γ_{real}) which are then smoothed using a Gaussian kernel with $\sigma_M(M)$. The output is fitted using χ^2 minimization and the corresponding fitted value of the slope (which we will call γ_{fit}) is obtained. Finally, as shown in Fig. 5, a polynomial is fit to $\gamma_{\text{fit}} - \gamma_{\text{real}}$ as a function of γ_{fit} which is the correction that needs to be applied. Note that since $\sigma_M(M)$ is data-dependent, an individual correction has to be applied to each specific observation.

We show in Fig. 5 the correction for the specific case of the NGC 4214 data previously mentioned. The magnitude of the correction can be taken to be typical for HST photometry beyond the Magellanic Clouds obtained with a few orbits of exposure time. The bias produced by not applying the correction is in the same direction as the one caused by constant-size bins: the measured IMF appears to be flatter than the real one.

We recommend that the correction described here be applied to the calculation of IMFs in general. However, we should point out that, ideally, one would like the correction to be as small as possible. One (obvious) way to achieve this is to obtain photometry with better S/N ratio. Another one is to use as many filters as possible to adequately characterize the temperature (and possibly gravity and metallicity) of each star and to adequately correct for extinction and then to process the data using a code like CHORIZOS, instead on relying on conversions from single-color + magnitude diagrams to temperature + luminosity equivalents.

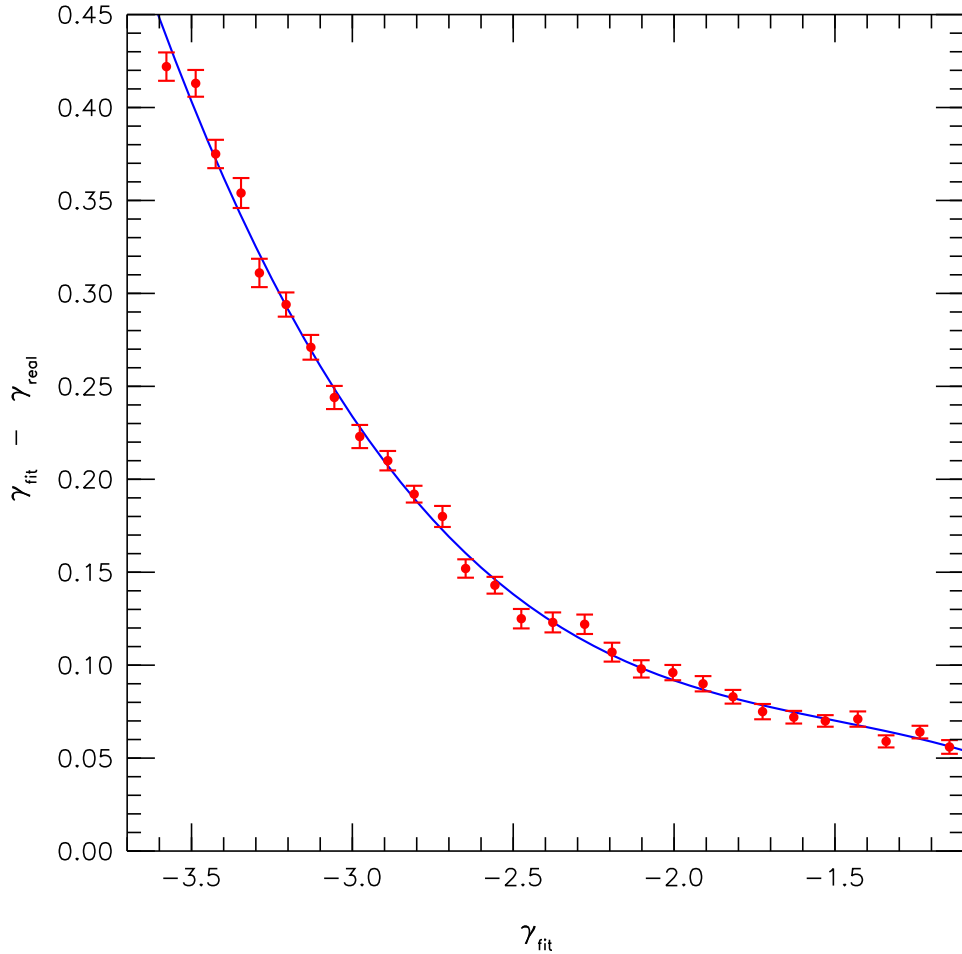


Figure 5. Correcting mass-diffusion biases. The plot shows the difference between the fitted and the real slopes of the IMF as a function of the fitted value for the artificial IMF realizations described in the text. The individual data points are the results of the fit to the realizations and the continuous line is a polynomial fit. The $\sigma_M(M)$ and the total number of stars used are those corresponding to the NGC 4214 data of Úbeda et al. (2005).

4. Multiplicity

The third type of bias that will be discussed here is that caused by multiplicity. It has been known for a long time that a large fraction of stars are located in multiple systems. For example, Kouwenhoven *et al.* (2005) measured that at least 61% of the stars in the Scorpius-Centaurus OB association are in a multiple system (the number could actually be higher due to incompleteness and selection effects). Interestingly, the single-star fraction decreases for early spectral types: those authors measured that 41% of the systems in which the primary is a B4-B9 are single but the fraction decreases to 12% if the primary is a B1-B3. The large multiplicity at the high-mass end of the stellar mass spectrum is not a new result: Mason *et al.* (1998) measured that at least 75% of the stellar systems with O stars in clusters or associations are multiple. Furthermore, those authors recognized that with the current instrumentation capabilities there is still enough discovery space between visual and spectroscopic binaries to allow for basically all O stars in clusters and associations to be part of multiple systems.

The existence of unresolved binaries artificially flattens the IMF due to a combination of two effects. First, an unresolved binary of any mass is shifted from a lower mass to a higher mass in a mass histogram. Second, the flattening should be further enhanced by the apparent increase of multiplicity with mass in the range between a few and several tens of solar masses, which is the range for which Salpeter slopes are reported by most authors (Chabrier 2003 and references therein).

The flattening due to unresolved binaries has been estimated by Kroupa (2001) to produce a change in γ between 0.0 and 1.3 for low-mass stars and brown dwarfs. Given the large multiplicity fractions observed for OB stars, the effect must also be significant for intermediate- and high-mass stars. At the highest end of the stellar mass spectrum, the problem of the calculation of the IMF slope is coupled with another one: is there an upper limit for stellar masses or is the highest mass in a cluster simply determined by statistical sampling in a quasi-Salpeter power law that extends to infinite masses? A few years ago there was a large discrepancy between the highest mass measured from orbital motion (the most reliable method of measuring masses), which yielded values around $60 M_{\odot}$, and the masses measured from photometry and spectral classification in R136 by Massey & Hunter (1998). Those authors measured stellar masses in the range $120-150 M_{\odot}$ and claimed that the data were compatible with a Salpeter IMF that extended beyond there. That gap has been recently narrowed in both directions. On the one hand, the $60 M_{\odot}$ barrier for spectroscopic-binary masses has been broken and the current heavyweight champion, WR 20a, lies around $80 M_{\odot}$ (Rauw *et al.* 2004; Bonanos *et al.* 2004). On the other hand, new statistical analyses indicate that there appears to be an upper mass limit somewhere in the $120-200 M_{\odot}$ range (Weidner & Kroupa 2004; Oey & Clarke 2005; Figer 2005).

In order to study the effect of unresolved binaries on the slope of the IMF at its upper-mass end and to obtain a better constraint on the stellar upper mass limit, we are currently engaged in an HST GO program (10602) which is a continuation of a previous one (10205). We are obtaining multi-filter imaging of all known Galactic O2/O3/O3.5 stars with the High Resolution Channel (HRC) on the Advanced Camera for Surveys (ACS). The HRC has a pixel size of $0''.027$ and

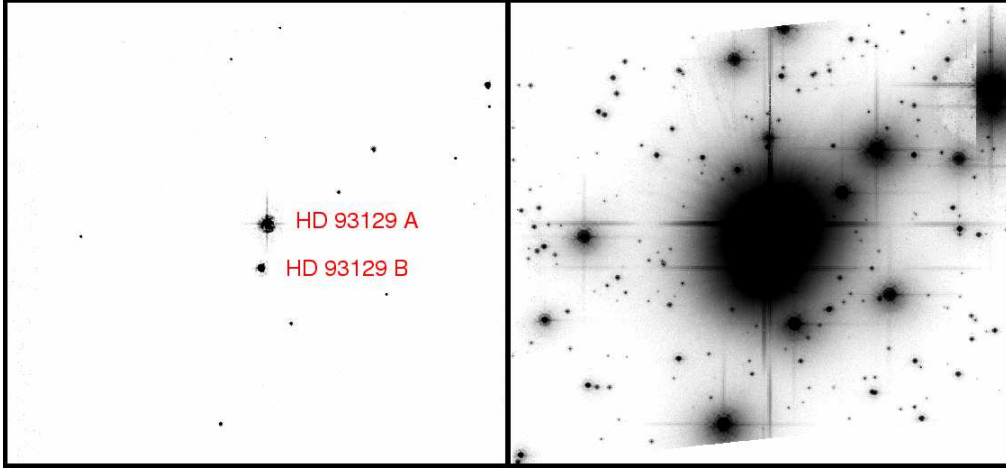


Figure 6. HRC images of the core of Trumpler 14. The left panel shows the F435W (*B*) image and the right panel shows the F850LP (*z*) image. The field size is $31.0'' \times 28.6''$. Top is 23.2 degrees West of North. Geometric distortion has been removed from the images but some cosmetic artifacts are still present in the F850LP case.

its PSF is well sampled and very stable across the detector (Anderson & King 2004). Furthermore, its geometric distortion is very well characterized, allowing for a relative astrometric precision of 0.005 pixels for very bright stars.

We present here our first results on the core of Trumpler 14 (Fig. 6), a young cluster in the Carina Nebula Association that contains at least three very-early O-type stars, including HD 93129 A, of spectral type O2 If*, the closest known O2 star (Walborn et al. 2002; Maíz Apellániz et al. 2004), and HD 93129 B, which is an O3.5 V((f+)). Those two stars are separated by $2''.7$ and appeared to be single in ground-based speckle interferometry (Mason et al. 1998). Recently, however, Nelan et al. (2004) were able to split HD 93129 A into two components using the Fine Guidance Sensor (FGS) on HST. They obtained a separation of 55 ± 3 mas at a position angle of 356 ± 4 degrees (measured from N towards E) and a magnitude difference of 0.90 ± 0.05 in the visible. In the same data HD 93129 B is unresolved.

We applied a PSF-fitting IDL photometry code especially written for this purpose to the HRC data for HD 93129 A and B. The code was applied to two dithered exposures in each of the F220W and F435W filters, thus yielding four independent measurements for each star. If a single component is used for the fit, the residuals for HD 93129 B are very small but those of HD 93129 A are very large, as expected for a binary system (Figs. 7 and 8). On the other hand, a two-component fit yields very small residuals for HD 93129 A, hence confirming the binary character detected with FGS.

We present the results of the two-component PSF fitting to HD 93129 A in Table 3. The final row shows the proposed values for the separation, position angle, and Δm derived from the four independent HRC exposures. Our position angle is 18 ± 4 degrees to the E of that measured by Nelan et al. (2004), suggesting that we are detecting the relative motion of HD 93129 Ab with respect

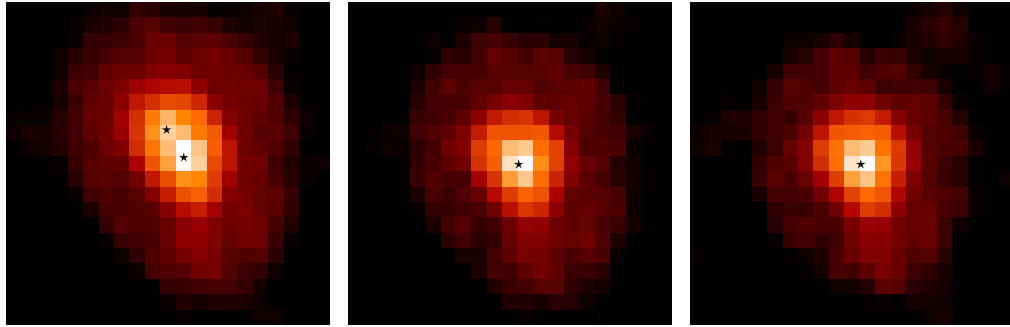


Figure 7. Postage stamps extracted from one of the two F435W HRC exposures for the two main components of HD 93129 (A, left and B, center) and PSF used for fitting (right). A logarithmic scale between 0.1% and 100% of the peak value is used in all cases. The field size is $0''.53 \times 0''.53$. Star symbols are used to identify the positions obtained by PSF fitting.

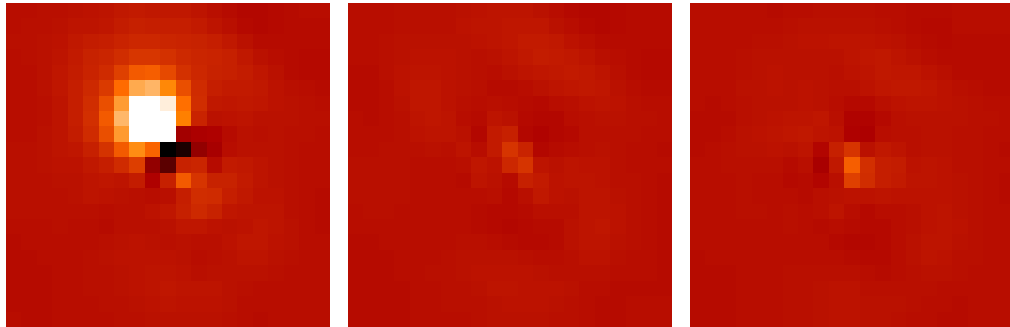


Figure 8. Fit residuals for HD 93129 A (left and center) and HD 93129 B (right) for one of the F435W exposures. The central panel assumes two components (e.g. it treats A as a binary system) while the other two assume a single component. A linear scale between -3% and 3% of the peak value for the data is used in all cases. The residuals have been smoothed with the PSF. The field size is $0''.53 \times 0''.53$.

Table 3. PSF analysis for the two components of HD 93129 A.

	Separation (mas)	Position angle ($^{\circ}$)	Δm
F220W exp. 1	50.4 ± 2.5	16.8 ± 2.8	1.1589 ± 0.0087
F220W exp. 2	51.4 ± 2.5	13.3 ± 2.7	1.1751 ± 0.0086
F435W exp. 1	52.0 ± 2.5	14.4 ± 2.7	1.1284 ± 0.0055
F435W exp. 2	52.1 ± 2.5	13.2 ± 2.7	1.1244 ± 0.0052
Final value	51.5 ± 1.2	14.4 ± 1.4	1.1670 ± 0.0061 (F220W) 1.1263 ± 0.0038 (F435W)

to Aa. From the 2.4 year difference between the epochs of the FGS and HRC observations we derive a very preliminary orbital period of \sim 50 years for the system but, obviously, observations at other epochs will be needed to confirm and measure an orbit. We point out that this is the first O2/O3/O3.5 star ever measured to be an astrometric binary.

The magnitude difference between HD 93129Aa and Ab measured from the HRC data is similar to but slightly larger than the one measured with FGS (which uses light with longer wavelengths). The two components have very similar F220W-F435W colors, with Ab being redder only by 0.0407 ± 0.0072 magnitudes. Given their proximity, it appears unlikely that the relative color is caused by differences in the amount or type of extinction. On the other hand, such a difference in color is equivalent to that between 50 000 K and 44 000 K for TLUSTY models (Lanz & Hubeny 2003) with $\log g = 4.75$ and solar metallicity, indicating that both components are likely to be early-O stars. We are currently working on a more detailed analysis of the photometry using CHORIZOS (Maíz Apellániz 2004).

It is important to note that HD 93129 A has not been identified as a spectroscopic binary. With a separation between its two components of about 150 AU, one would expect relative velocities of the order of 30 km s^{-1} if the inclination is large. Therefore, its non-identification is not surprising, since one would require a separation an order of magnitude smaller to allow for a clear detection of radial velocity variations¹ (see e.g. Bonanos & Stanek 2005). This also means that we cannot even discard the possibility that either HD 93129 Aa or Ab are binaries themselves.

What does this mean for the biases in the top end of the IMF induced by multiplicity? Trumpler 14 is at an approximate distance of 2.7 kpc. If it were located at the same distance as the Galactic Center or NGC 3603, HD 93129 A will likely appear unresolved with HRC or FGS. At the distance of the Magellanic Clouds, Aa and Ab would be unresolved and A and B could be resolved but only with HST or adaptive optics. Moving to M31 or M33, HD 93128 (another O3 star in the cluster outside the field in Fig. 6) and HD 93129 would have an angular separation similar to that of Aa and Ab at its actual distance, with the rest of the stars (likely of late-O and B type) in Fig. 6 in between. This yields a total of (at least) four early-type stars blended together in a cluster that is quite massive, but far less than R136. The reader can easily deduce from these simple calculations how much he/she can trust IMF derivations of extragalactic young clusters that do not take into account multiplicity corrections.

5. Conclusions

We have discussed three sources of biases in the determination of the initial mass function (IMF): [1] the use of constant-size bins, [2] the uncertainty in the determinations of masses, and [3] the existence of unresolved multiple systems. Those three effects tend to produce IMFs that are flatter than the real one, all

¹Of course, close binaries are easier to detect not only because the radial velocity variations are larger but because they occur on shorter time scales.

of them large enough to potentially introduce significant systematic errors in the derived power-law slope. In the first case we present a technique that can get rid of the bias almost completely, even after the data have been obtained. In the second case we present a method that can also be used a posteriori to estimate the biases and we give some advice as to how to reduce them by using multifilter data. The third case, as demonstrated by the example of HD 93129 A, is harder to correct, given that the current capabilities do not allow us to detect all multiple systems in the stellar clusters and associations of interest, even those in our own Galaxy. Nevertheless, that should not preclude us from making an effort to close the current gap between visual and spectroscopic binaries or from trying to estimate the contribution of unresolved multiple systems to the IMF slope.

Acknowledgments. Support for this work was provided by NASA through grants GO-09419.01, AR-09553.02, and GO-10205.01 from the Space Telescope Science Institute, Inc., under NASA contract NAS5-26555.

References

Anderson, J., & King, I. R. 2004, ACS Instrument Science Report 2004-15
 Bonanos, A. Z., & Stanek, K. Z. 2005, in ASP Conference Series, Vol. 332, 257
 Bonanos, A. Z., et al. 2004, ApJL, 611, L33
 Chabrier, G. 2003, PASP, 115, 763
 Dolphin, A. E. 2000, PASP, 112, 1383
 Fall, S. M., & Zhang, Q. 2001, ApJ, 561, 751
 Figer, D. F. 2005, Nature, 434, 192
 Kouwenhoven, M. B. N., Brown, A. G. A., Zinnecker, H., Kaper, L., & Portegies Zwart, S. F. 2005, A&A, 430, 137
 Kroupa, P. 2001, MNRAS, 322, 231
 Lanz, T., & Hubeny, I. 2003, ApJS, 146, 417
 Lucy, L. B. 2000, MNRAS, 318, 92
 Maeder, A., & Meynet, G. 2001, A&A, 373, 555
 Maíz Apellániz, J., Walborn, N. R., Galué, H. Á., & Wei, L. H. 2004, ApJS, 151, 103
 Maíz Apellániz, J. 2004, PASP, 116, 859
 Maíz Apellániz, J., & Úbeda, L. 2005, ApJL (20 August 2005 issue)
 Mason, B. D., Gies, D. R., Hartkopf, W. I., Bagnuolo, W. G., Brummelaar, T. T., & McAlister, H. A. 1998, AJ, 115, 821
 Massey, P., & Hunter, D. A. 1998, ApJ, 493, 180
 Nelan, E. P., Walborn, N. R., Wallace, D. J., Moffat, A. F. J., Makidon, R. B., Gies, D. R., & Panagia, N. 2004, AJ, 128, 323
 Oey, M. S., & Clarke, C. J. 2005, ApJL, 620, L43
 Rauw, G., et al. 2004, A&A, 420, L9
 Stetson, P. B. 1987, PASP, 99, 191
 Úbeda, L., Maíz Apellániz, J., & MacKenty, J. W. 2005, in preparation
 Walborn, N. R., et al. 2002, AJ, 123, 2754
 Weidner, C., & Kroupa, P. 2004, MNRAS, 348, 187
 Wheaton, W. A., Dunklee, A. L., Jacobsen, A. S., Ling, J. C., Mahoney, W. A., & Radocinski, R. G. 1995, ApJ, 438, 322